



Rayleigh-wave phase-velocity azimuthal anisotropy beneath western Canada

Xuewei Bao^{a*}, David W. Eaton^a, Yu Jeffrey Gu^b

^aDepartment of Geoscience, University of Calgary, Calgary, Alberta T2N 1N4, Canada

^bDepartment of Physics, University of Alberta, Edmonton, Alberta T6G 2E1, Canada

*Corresponding author:

Email address: xubao@ucalgary.ca (X.W. Bao), Tel.: +1 403 220 7923.

Abstract:

We present fundamental-mode Rayleigh-wave azimuthally anisotropic phase-velocity maps in the period range 20-150 s for western Laurentia and the southern Canadian Cordillera in western Canada. These maps offer new constraints on the depth distribution of seismic anisotropy in this region using data from several recent seismic arrays. At short periods (20-25 s), strong anisotropy with an orogen-parallel fast direction appears in the Cordillera and neighbouring foreland belt, suggesting pervasive ductile deformation in the lower crust during the Cordillera orogenesis. At periods of 70 s and higher, a zone of low-to-zero azimuthal anisotropy occurs in the southern part of the Cordillera, indicative of weak asthenospheric anisotropy likely due to some combined effects of slab window, lithospheric delamination and edge-driven convection. Depth-variant azimuthal anisotropy is also found beneath the cratonic part of the study region. The dominant directions of fast wave propagation in the southeastern part of the craton change from N-S at periods of <120 s to NE-SW at 150 s period, which is interpreted as evidence for different origins of the observed anisotropy with frozen-in anisotropy in the cratonic lithosphere and flow-driven anisotropy in the asthenosphere.

Keywords: Surface-wave tomography; seismic anisotropy; Cratons; Canadian Cordillera

1. Introduction

In response to the intensive tectonic strains through long periods of geological time, the intrinsically anisotropic crustal (e.g., mica and amphibole) and mantle (e.g., olivine and pyroxene) minerals could form preferred alignments that give rise to the detectable seismic anisotropy, that is, the direction or polarization dependence of seismic wavespeeds [Crampin *et al.*, 1984; Silver, 1996]. Seismic azimuthal anisotropy appears in various types of seismic data [Forsyth, 1975; Montagner and Tanimoto, 1991, Plomerov *et al.*, 2002; Savage, 1999; Shearer and Orcutt, 1986] and the fast direction of wave propagation has been widely used as an indicator of the directions of maximum deformation during the past and more recent tectonic events [Nicolas and Christensen, 1987]. In the lithospheric mantle, the lattice preferred orientation of olivine is often attributed to “frozen-in” fabric formed by past deformation processes [Ismail and Mainprice, 1998], whereas in the asthenosphere seismic anisotropy is usually related to present and recent mantle flow [Adam and Lebedev, 2012; Deschamps *et al.*, 2008; Marone and Romanowicz, 2007].

The most commonly used technique for investigating seismic azimuthal anisotropy beneath continent is shear-wave splitting [Savage, 1999], which provides high lateral resolution but poor vertical resolution due to the near-vertical ray path. As a consequence, the interpretation of shear-wave splitting observations is controversial [Savage, 1999;

Jeff Gu 2015-7-7 3:05 PM




Deleted: some

Unknown

Field Code Changed

Jeff Gu 2015-7-7 3:05 PM

Formatted: Font:Not Italic

Silver, 1996]. In some regions, the fast-propagation azimuths from shear-wave splitting follow regional tectonic structure,  indicative of a lithospheric origin, while other regions show large scale coherent fast-propagation directions that parallel to those of the absolute plate motion, suggesting an asthenospheric origin [Vinnik *et al.*, 1992][[Bockleman and Silver study](#)].  Surface waves can offer the much needed vertical resolution to provide essential constraints on the depth distribution of seismic anisotropy [Gaherty, 2004; Montagner and Tanimoto, 1991]. Global and continental scale tomographic models from surface wave modelling have depicted different patterns of azimuthal anisotropy in the continental lithosphere and asthenosphere  [Debayle *et al.*, 2005; Marone and Romanowicz, 2007; Montagner and Tanimoto, 1991; Yuan and Romanowicz, 2010]. Regional-scale studies using surface wave data from dense broad-band arrays have been producing increasingly high resolution 3-D models of anisotropy and thus significantly improving our understanding of continental deformation [Chen *et al.*, 2015; Darbyshire *et al.*, 2013; Darbyshire and Lebedev, 2009; Fry *et al.*, 2010; Li *et al.*, 2003; Lin *et al.*, 2011; Pawlak *et al.*, 2012; Pedersen *et al.*, 2006; Yao *et al.*, 2010].

In the current study, we present azimuthally anisotropic Rayleigh-wave phase-velocity maps for western Canada. The tectonics of western Canada is characterized by a transition from the Phanerozoic Cordilleran orogen in the west to the Precambrian craton in the east (Figure 1), making this region an excellent natural laboratory to study continental dynamics in terms of cratonic evolution and plateau deformation. The eastern

part of our study region belongs to Laurentia, the continental nucleus of North America. The assembly of this part of Laurentia is thought to have occurred in the ca. 2.0-1.8 Ga timeframe through a series of complex processes that evolved plate collision and/or terrane accretion among the diverse domains [Hoffman, 1988; Ross, 2002]. Following the assembly of these Precambrian domains, a thick Proterozoic passive-margin sequence developed along the western flank of Laurentia. This margin was further modified by tectonic accretion and orogenic activity in the Canadian Cordillera since the Jurassic [Cook, 1995].

The rich tectonic history of this region has inspired a lot of geophysical studies. The intricate crustal domains in the east buried beneath the West Canada Sedimentary Basin (Figure 1) and their relationships have been examined since about three decades ago by analysis of regional gravity and magnetic field, seismic reflection and refraction profiles and geochronological data [Ross *et al.*, 1991, 2000; Ross, 2002; and references therein]. These efforts are considerably complemented by a variety of passive seismological studies and magnetotelluric surveys, which provide more constraints on the heterogeneities of the lithosphere-asthenosphere system beneath western Canada [Bao and Eaton, 2015; Bao *et al.*, 2014; Boerner *et al.*, 1999; Cassidy, 1995; Dalton and Gaherty, 2013; Dalton *et al.*, 2011; Gu and Shen, 2015; Gu *et al.*, 2015; Kao *et al.*, 2013; Mercier *et al.*, 2009; Nieuwenhuis *et al.*, 2014; Shragge *et al.*, 2002]. However, the azimuthal anisotropic information on the deep structure of the study area has only been

studied by a few SKS-splitting observations [Courtier *et al.*, 2010; Currie *et al.*, 2004; Shragge *et al.*, 2002; Zalt *et al.*, 2009]. The Rayleigh wave azimuthal anisotropy at different periods obtained in this paper provides the complementary knowledge on the depth distribution of anisotropy to further our understanding of the complicated geodynamic processes in western Canada.

2. Data set and Tomographic inversion

Fundamental-mode Rayleigh wave data utilized in this study are from 19 stations of the Canadian National Seismograph Network (CNSN), 9 stations of the Alberta Telemetered Seismograph Network (ATSN), 19 stations of the Canadian Rockies and Alberta Network (CRANE) [Gu *et al.*, 2011], and 39 stations from USArray (Figure 1). We selected 583 shallow and intermediate-focus events (depths < 100 km) in a distance range of 20°-120° with magnitude larger than 6 in the 2006 to 2013 time period. The inter-station Rayleigh-wave phase-velocity dispersion curves were extracted from high-quality records using a cross-correlation method [Bao *et al.*, 2011; Yao *et al.*, 2006]. The two-station cross-correlation method can remove path effects between the earthquake source and the seismograph network and the influence due to the errors of source parameters, and is, therefore, a powerful tool for regional studies of the lithosphere and asthenosphere structure [Yao *et al.*, 2006]. The number of Rayleigh-wave phase-velocity measurements varies with period with a maximum of ~1400 at 50 s period. The detailed descriptions of

the data analysis are given in two relevant papers [Bao and Eaton, 2015; Bao et al., 2014] and will not be repeated here.

From the resulting dispersion data, we used a linearized 2D inversion method [Bao et al., 2013; Xu et al., 2013] to construct phase-velocity maps at $1^\circ \times 1^\circ$ grid spacing for the study region. Using ray theory, for each inter-station path, the predicted frequency-dependent travel time $t(\omega)$ was obtained from the measured phase-velocity distribution $c(\theta, \phi, \omega)$

$$t(\omega) = \int c^{-1}(\theta, \phi, \omega) ds, \quad (1)$$

where ω is frequency and θ, ϕ specify coordinates of the geographical points along the path. The inversion problem can be expressed in the form of $\mathbf{Gm} = \mathbf{d} + \mathbf{e}$, where the vector \mathbf{d} contains the observed travel-time residuals relative to the reference model (usually the average phase velocity at each period) and the vector \mathbf{m} denotes the model parameters (isotropic phase velocities and azimuthally anisotropic coefficients). The sensitivity matrix \mathbf{G} is known from the forward problem. To estimate \mathbf{m} we minimized the following objective function

$$E = \|\mathbf{Gm} - \mathbf{d}\|^2 + \lambda^2 \|\mathbf{m}\|^2 + \phi^2 \|\mathbf{Lm}\|^2. \quad (2)$$

The first term in eq. (2) measures the data misfit; the second is a model regularization term; and the third term is a Laplacian smoothing constraint, where L is the 2D finite-difference Laplacian operator, and λ and ϕ are the damping and smoothing factors, respectively. User-defined regularization parameters were selected based on a series of tests. The parameter λ constrains the inversion in order to reduce deviation from the a

priori velocity model, such that a large value of λ results in small perturbations. Similarly, a larger ϕ results in a smoother model. We selected values for λ and ϕ that, in our experience, appropriately balance the data misfit, model damping, and smoothness. The resulting sparse system of equations was solved using the LSQR algorithm [Paige and Saunders, 1982].





To solve for azimuthal anisotropy, we can express Rayleigh-wave phase velocity c as a function of azimuth ψ :

$$c(\theta, \phi, \omega) = A_0(\omega) + A_1(\omega) \cos(2\psi) + A_2(\omega) \sin(2\psi) + A_3(\omega) \cos(4\psi) + A_4(\omega) \sin(4\psi) \quad (3)$$

where A_0 is the azimuthal averaged phase velocity and A_1 - A_4 are azimuthal anisotropic coefficients [Smith and Dahlen, 1973]. We can ignore the 4ψ terms because they are very small [Li *et al.*, 2003; Montagner and Nataf, 1986; Yao *et al.*, 2010]. The peak-to-peak amplitude of anisotropy is expressed as $2\sqrt{(A_1^2 + A_2^2)}/A_0$, and the fast wave propagation direction is represented as $\arctan(A_2/A_1)/2$.

3. Results

In order to test the robustness of the anisotropic results, a series of synthetic tests were performed. First, we created a purely isotropic checkerboard model, consisting of alternating positive and negative anomalies with magnitude of 5 % above or below the average phase velocity at the corresponding period, respectively. Synthetic phase-velocity data were calculated according to the actual inter-station path, and 2.5% random error in

phase velocity was added to mimic the errors in real data. These data were then used as input to the same inversion procedure described above, using of the same damping and smoothing parameters. Figure 2 shows that the checkerboard velocity pattern is generally well recovered. An important element of this test is to show that the leakage of the anisotropy into the model is weak. The spurious anisotropy shows strong lateral variation and is approximately less than 1% in magnitude. Second, a checkerboard anisotropic model was created with the fast azimuthal axis oriented NE-SW and NW-SE for Rayleigh waves, from which synthetic phase-velocity data were calculated as  did above. The anisotropic patterns for Rayleigh waves are generally reconstructed (Figure 3). To examine further the robustness of the models and the leakage between isotropic and anisotropic structure, we took a phase-velocity map obtained from the Rayleigh-wave data set at a period of 70 s, removed either the isotropic or anisotropic part, and then reinverted it. Reconstruction results show that, in general, the leakage between isotropic phase velocity and anisotropic parameters was  (Figure 4). It is also clear that the artificial anisotropy caused by the leakage of the isotropic heterogeneity shows rapid variations in contrast to the smooth distributions of anisotropy  that we imaged  which suggests that the effect of the trade-offs on the imaged anisotropy is likely to be limited.

In Figure 5, we represented the azimuthally anisotropic phase-velocity maps at periods from 25 to 150 s, which are sensitive to the velocity structure in a depth range from the lower crust to the uppermost mantle. Throughout the period range considered here, the

striking feature of the isotropic velocity distribution is the pronounced structural transition from the high velocities within the craton in the northeast to the much lower velocities beneath the Cordillera in the southwest. This regional pattern of isotropic velocity distribution is similar to our previous models from isotropic tomography inversion, suggesting that the isotropic phase velocities do not significantly depend on whether azimuthal anisotropy was taken into account in the inversions.

Figure 5 also displays the pronounced variations of azimuthal anisotropy with period in our model. At short periods (25 s) that mainly sample the lower crust, we observe an orogen-parallel fast direction (nearly NW-SE) in the Canadian Cordillera and the neighbouring foreland belt, where the peak-to-peak magnitude of anisotropy is the strongest (up to 4%). However, the azimuth anisotropy tends to fade obviously to the interior of the craton at this period, forming a zone of low-to-null azimuthal anisotropy in the east. At intermediate periods (40 s and 50 s) primarily sampling the uppermost mantle, the eastern part of the craton is characterized by relatively weak anisotropy, trending in an N-S fast-propagation direction. At these periods, the southern part of the Canadian Cordillera shows a noticeable decrease in the anisotropy amplitude and changes of the fast Rayleigh wave propagation direction to nearly N-S. At long periods (70 s and 90 s), the peak-to-peak anisotropy increases to 2.0%-2.5% in the southeastern craton region, reflecting the stronger shear velocity azimuthal anisotropy in the middle lithosphere. The N-S trending azimuthal anisotropy of the southeastern craton persists to

periods of 100 and 120 s, corresponding to the depth range of the mid-lower lithosphere under the craton.

On the other hand, a zone of nearly low-to-zero azimuthal anisotropy appears in the southern Canadian Cordillera at periods of 70 s and more, indicating the weaker shear velocity azimuthal anisotropy in the asthenosphere because of its much thinner lithosphere beneath the Cordillera [Bao *et al.*, 2014]. At periods of 150 s that increasingly sample the asthenosphere beneath the craton, the fast-propagation directions in the southeastern craton change towards NE-SW.

4. Discussion

One of the most striking features of our model is the strong orogen-parallel anisotropy around the lower crustal depth beneath the Canadian Cordillera and the neighbouring foreland belt. The NW-SE trending strong anisotropy is perpendicular to the regional maximum horizontal compressional stress [Reiter *et al.*, 2014] and indicates the pervasive deformation in the lower crust outboard of the craton. The main sources for crustal anisotropy include shape-preferred orientation (SPO) of cracks in the upper crust and lattice preferred orientation (LPO) of anisotropic crustal minerals (e.g., mica and amphibole) in the mid-lower crust due to intensive, regionally coherent strain [Crampin *et al.*, 1984]. Thus the strong anisotropy in the lower crust we imaged here is likely to be caused by LPO of amphibole and/or mica formed during past tectonic events. Since the Jurassic, the Cordilleran orogenesis has dominated the tectonic evolution to the west

[Cook, 1995], which was initiated by the oblique plate convergence along the western margin of North America. The accompanying compression stress field may probably have aligned LPO of amphibole and/or mica in the lower crust perpendicular to the direction of the regional stress, manifested as the orogen-parallel anisotropy we observed in this study. Similar orogen-parallel anisotropy have been detected in several previous works. For instance, *Fry et al.* [2010] imaged pervasive orogen-parallel anisotropy above 30 km in the central Alps using ambient noise tomography. With surface wave tomography, *Deschamps et al.* [2008] found that directions of fast wave propagation in the upper lithosphere (30-70 km depths) beneath the east-central United States are parallel to the Grenville and Appalachian fronts. The pervasive orogen-parallel deformation fabrics observed by these studies suggest that broad continuously distributed deformation may be a common phenomenon in continental collision zones, which occurs not only in the upper crust [*Zhang et al.*, 2004] but also in the mid-lower crust likely through ductile flow.

Another pronounced feature of our results is the low-to-zero azimuthal anisotropy in the asthenosphere beneath the southern Canadian Cordillera. The weak azimuthal anisotropy from our surface wave tomography agrees well with the null-splitting measurements of SKS-splitting [*Currie et al.*, 2004], which may be ascribed to a regional vertical mantle flow. The possible causes for the vertical mantle flow in this region may include the delamination of lithospheric mantle, slab window and edge-driven convection. Based on surface wave tomography, the rapid uplift of the southern

Canadian Cordillera has been interpreted as the result of lithospheric delamination [Bao *et al.*, 2014], which may shift fast seismic velocity direction from horizontal to vertical, as shown in the Great Basin region [West *et al.*, 2009]. In addition, slab window-induced asthenospheric flow has also been proposed to explain the null splitting observation [Zandt *et al.*, 2009] and intraplate volcanism [Thorkelson *et al.*, 2011] in the Canadian Cordillera. Furthermore, the vertical flow component of the edge-driven convection [Hardebol *et al.*, 2012] caused by the sharp change of lithospheric thickness from the Cordillera to the craton may also contribute to the weak azimuthal anisotropy. Thus the different patterns of azimuthal anisotropy at different depth (periods) in the Cordillera reflect the impacts of its complex tectonic evolution.

Depth-variant azimuthal anisotropy also seems to appear in the eastern part of the craton region. At periods sampling the upper-middle cratonic lithosphere (40 - 120 s), the dominant directions of fast wave propagation are N-S, whereas at a period of 150 s sampling the lower lithosphere and asthenosphere, the fast wave azimuths change towards NE-SW close to the absolute plate motion of the North American plate. Previous shear wave splitting measurements also suggested the existence of multiple layers of anisotropy in this region. Significant azimuthal variations in the shear wave splitting parameters with a 90° periodicity were observed in the two stations (WALA and EDM, as shown in Fig. 1), which is indicative of layered anisotropy [Currie *et al.*, 2004]. Further modeling by Currie et

al. [2004] suggested an upper layer of anisotropy with a nearly N-S fast direction ($N12^{\circ}E$) and a lower layer of anisotropy with a fast direction of $N81^{\circ}E$, which is broadly coincident with the depth variation of Rayleigh wave azimuthal anisotropy revealed in this study. Two layers of anisotropy beneath the North American craton has also been imaged by other continental and regional scale tomography studies [Darbyshire and Lebedev, 2009; Yuan and Romanowicz, 2010], with the upper layer of “frozen-in” anisotropy and the lower layer of anisotropy caused by recent and present-day mantle flow.

5. Conclusions

The depth distribution of azimuthal anisotropy in western Canada was obtained through regional Rayleigh-wave tomography for the first time. Our azimuthally anisotropic phase-velocity maps reveal a pronounced orogen-parallel anisotropy in the Cordillera and its foreland belt at short periods mainly sampling the lower crust. This together with other similar observations supports pervasive ductile deformation in continental collision zones. A zone of low-to-zero azimuthal anisotropy in the southern part of the Cordillera appears in the periods sampling the asthenosphere there, which is likely due to the complex vertical asthenospheric flow pattern caused by the combined effects of slab window, lithospheric delamination and edge-driven convection. The southeastern part of the craton is characterized by two layers of anisotropy with seismic fast directions of nearly N-S at periods of <120 s mainly

sampling the lithosphere and fast azimuths of NE-SW at a period of 150 s penetrating into the asthenosphere. This is consistent with SKS-splitting observation, probably indicating the “frozen-in” anisotropy in the cratonic lithosphere and the asthenospheric anisotropy formed by the shear deformation of present-day and recent mantle flow.

Acknowledgements:

Seismic data were provided by the Incorporated Research Institutions for Seismology Data Management Center and the Canadian National Data Center. This study was funded by a grant to DWE from the Natural Sciences and Engineering Research Council of Canada (NSERC). Most figures were produced using Generic Mapping Tools (GMT) (Wessel and Smith, 1998). We thank the team of CRANE project for the hard work to collect their data.

References:

- Adam, J. M. C., and S. Lebedev (2012), Azimuthal anisotropy beneath southern Africa from very broad-band surface-wave dispersion measurements, *Geophysical Journal International*, 191(1), 155-174, doi:10.1111/j.1365-246X.2012.05583.x.
- Bao, X., and D. W. Eaton (2015), Large variations in lithospheric thickness of western Laurentia: Tectonic inheritance or collisional reworking?, *Precambrian Research*(0), doi:<http://dx.doi.org/10.1016/j.precamres.2015.05.010>.

- Bao, X., D. W. Eaton, and B. Guest (2014), Plateau uplift in western Canada caused by lithospheric delamination along a craton edge, *Nature Geosci*, 7(11), 830-833, doi:10.1038/ngeo2270
- Bao, X., X. Song, M. Xu, L. Wang, X. Sun, N. Mi, D. Yu, and H. Li (2013), Crust and upper mantle structure of the North China Craton and the NE Tibetan Plateau and its tectonic implications, *Earth and Planetary Science Letters in press*.
- Bao, X., M. Xu, L. Wang, N. Mi, D. Yu, and H. Li (2011), Lithospheric structure of the Ordos Block and its boundary areas inferred from Rayleigh wave dispersion, *Tectonophysics*, 499(1-4), 132-141, doi:<http://dx.doi.org/10.1016/j.tecto.2011.01.002>.
- Boerner, D. E., R. D. Kurtz, J. A. Craven, G. M. Ross, F. W. Jones, and W. J. Davis (1999), Electrical Conductivity in the Precambrian Lithosphere of Western Canada, *Science*, 283(5402), 668-670, doi:10.1126/science.283.5402.668.
- Cassidy, J. F. (1995), Review: Receiver function studies in the southern Canadian Cordillera, *Canadian Journal of Earth Sciences*, 32(10), 1514-1519, doi:10.1139/e95-123.
- Chen, H., L. Zhu, Q. Ye, Q. Wang, Y. Yang, and P. Zhang (2015), Azimuthal anisotropy of the crust and uppermost mantle in northeast North China Craton from inversion of Rayleigh wave phase velocity, *Geophysical Journal International*, 202(1), 624-639, doi:10.1093/gji/ggv153.
- Cook, F. A. (1995), Lithospheric processes and products in the southern Canadian

- Cordillera: a Lithoprobe perspective, *Canadian Journal of Earth Sciences*, 32(10), 1803-1824, doi:10.1139/e95-139.
- Courtier, A. M., J. B. Gaherty, J. Revenaugh, M. G. Bostock, and E. J. Garnero (2010), Seismic anisotropy associated with continental lithosphere accretion beneath the CANOE array, northwestern Canada, *Geology*, 38(10), 887-890, doi:10.1130/g31120.1.
- Crampin, S., E. M. Chesnokov, and R. G. Hipkin (1984), Seismic anisotropy — the state of the art: II, *Geophysical Journal of the Royal Astronomical Society*, 76(1), 1-16, doi:10.1111/j.1365-246X.1984.tb05017.x.
- Currie, C. A., J. F. Cassidy, R. D. Hyndman, and M. G. Bostock (2004), Shear wave anisotropy beneath the Cascadia subduction zone and western North American craton, *Geophysical Journal International*, 157(1), 341-353, doi:10.1111/j.1365-246X.2004.02175.x.
- Dalton, C. A., and J. B. Gaherty (2013), Seismic anisotropy in the continental crust of northwestern Canada, *Geophysical Journal International*, 193(1), 338-348, doi:10.1093/gji/ggs108.
- Dalton, C. A., J. B. Gaherty, and A. M. Courtier (2011), Crustal VS structure in northwestern Canada: Imaging the Cordillera-craton transition with ambient noise tomography, *Journal of Geophysical Research: Solid Earth*, 116(B12), n/a-n/a, doi:10.1029/2011JB008499.
- Darbyshire, F. A., D. W. Eaton, and I. D. Bastow (2013), Seismic imaging of the

- lithosphere beneath Hudson Bay: Episodic growth of the Laurentian mantle keel, *Earth and Planetary Science Letters*, 373(0), 179-193, doi:<http://dx.doi.org/10.1016/j.epsl.2013.05.002>.
- Darbyshire, F. A., and S. Lebedev (2009), Rayleigh wave phase-velocity heterogeneity and multilayered azimuthal anisotropy of the Superior Craton, Ontario, *Geophysical Journal International*, 176(1), 215-234.
- Debayle, E., B. Kennett, and K. Priestley (2005), Global azimuthal seismic anisotropy and the unique plate-motion deformation of Australia, *Nature*, 433(7025), 509-512, doi:http://www.nature.com/nature/journal/v433/n7025/supinfo/nature03247_S1.html.
- Deschamps, F., S. Lebedev, T. Meier, and J. Trampert (2008), Stratified seismic anisotropy reveals past and present deformation beneath the East-central United States, *Earth Planet Sc Lett*, 274(3-4), 489-498, doi:<http://dx.doi.org/10.1016/j.epsl.2008.07.058>.
- Forsyth, D. W. (1975), The Early Structural Evolution and Anisotropy of the Oceanic Upper Mantle, *Geophysical Journal of the Royal Astronomical Society*, 43(1), 103-162, doi:10.1111/j.1365-246X.1975.tb00630.x.
- Fry, B., F. Deschamps, E. Kissling, L. Stehly, and D. Giardini (2010), Layered azimuthal anisotropy of Rayleigh wave phase velocities in the European Alpine lithosphere inferred from ambient noise, *Earth Planet Sc Lett*, 297(1-2), 95-102,

doi:<http://dx.doi.org/10.1016/j.epsl.2010.06.008>.

Gaherty, J. B. (2004), A surface wave analysis of seismic anisotropy beneath eastern North America, *Geophysical Journal International*, 158(3), 1053-1066, doi:10.1111/j.1365-246X.2004.02371.x.

Gu, Y. J., A. Okeler, L. Shen, and S. Contenti (2011), The Canadian Rockies and Alberta Network (CRANE): New Constraints on the Rockies and Western Canada Sedimentary Basin, *Seismological Research Letters*, 82(4), 575-588, doi:10.1785/gssrl.82.4.575.

Gu, Y. J., and L. Shen (2015), Noise correlation tomography of Southwest Western Canada Sedimentary Basin, *Geophysical Journal International*, 202(1), 142-162, doi:10.1093/gji/ggv100.

Gu, Y. J., Y. Zhang, M. D. Sacchi, Y. Chen, and S. Contenti (2015), Sharp mantle transition from cratons to Cordillera in southwestern Canada, *Journal of Geophysical Research: Solid Earth*, n/a-n/a, doi:10.1002/2014JB011802.

Hardebol, N. J., R. N. Pysklywec, and R. Stephenson (2012), Small-scale convection at a continental back-arc to craton transition: Application to the southern Canadian Cordillera, *Journal of Geophysical Research: Solid Earth*, 117(B1), B01408, doi:10.1029/2011JB008431.

Hoffman, P. F. (1988), United Plates of America, The Birth of a Craton: Early Proterozoic Assembly and Growth of Laurentia, *Annual Review of Earth and Planetary Sciences*, 16(1), 543-603,

doi:doi:10.1146/annurev.ea.16.050188.002551.

Ismail, W. B., and D. Mainprice (1998), An olivine fabric database: an overview of upper mantle fabrics and seismic anisotropy, *Tectonophysics*, 296(1-2), 145-157, doi:[http://dx.doi.org/10.1016/S0040-1951\(98\)00141-3](http://dx.doi.org/10.1016/S0040-1951(98)00141-3).

Kao, H., Y. Behr, C. A. Currie, R. Hyndman, J. Townend, F.-C. Lin, M. H. Ritzwoller, S.-J. Shan, and J. He (2013), Ambient seismic noise tomography of Canada and adjacent regions: Part I. Crustal structures, *Journal of Geophysical Research: Solid Earth*, 118(11), 5865-5887, doi:10.1002/2013JB010535.

Li, A., D. W. Forsyth, and K. M. Fischer (2003), Shear velocity structure and azimuthal anisotropy beneath eastern North America from Rayleigh wave inversion, *J. Geophys. Res.*, 108, doi:10.1029/2002jb002259.

Lin, F.-C., M. H. Ritzwoller, Y. Yang, M. P. Moschetti, and M. J. Fouch (2011), Complex and variable crustal and uppermost mantle seismic anisotropy in the western United States, *Nature Geosci*, 4(1), 55-61, doi:<http://www.nature.com/ngeo/journal/v4/n1/abs/ngeo1036.html#supplementary-information>.

Marone, F., and B. Romanowicz (2007), The depth distribution of azimuthal anisotropy in the continental upper mantle, *Nature*, 447(7141), 198-201, doi:http://www.nature.com/nature/journal/v447/n7141/supinfo/nature05742_S1.html.

Mercier, J. P., M. G. Bostock, J. F. Cassidy, K. Dueker, J. B. Gaherty, E. J. Garnero, J.

- Revenaugh, and G. Zandt (2009), Body-wave tomography of western Canada, *Tectonophysics*, 475(3-4), 480-492, doi:<http://dx.doi.org/10.1016/j.tecto.2009.05.030>.
- Montagner, J.-P., and H.-C. Nataf (1986), A Simple Method for Inverting the Azimuthal Anisotropy of Surface Waves, *J. Geophys. Res.*, 91, doi:10.1029/JB091iB01p00511.
- Montagner, J.-P., and T. Tanimoto (1991), Global upper mantle tomography of seismic velocities and anisotropies, *Journal of Geophysical Research: Solid Earth*, 96(B12), 20337-20351, doi:10.1029/91JB01890.
- Nicolas, A., and N. I. Christensen (1987), Formation of Anisotropy in Upper Mantle Peridotites - A Review, in *Composition, Structure and Dynamics of the Lithosphere-Asthenosphere System*, edited, pp. 111-123, American Geophysical Union, doi:10.1029/GD016p0111.
- Nieuwenhuis, G., M. J. Unsworth, D. Pana, J. Craven, and E. Bertrand (2014), Three-dimensional resistivity structure of Southern Alberta, Canada: implications for Precambrian tectonics, *Geophysical Journal International*, 197(2), 838-859, doi:10.1093/gji/ggu068.
- Paige, C. C., and M. A. Saunders (1982), LSQR: An algorithm for sparse linear equations and sparse least squares, *TOMS*, 8(1), 43-71.
- Pawlak, A., D. W. Eaton, F. Darbyshire, S. Lebedev, and I. D. Bastow (2012), Crustal anisotropy beneath Hudson Bay from ambient noise tomography: Evidence for

- post-orogenic lower-crustal flow?, *Journal of Geophysical Research: Solid Earth*, 117(B8), n/a-n/a, doi:10.1029/2011JB009066.
- Pedersen, H. A., M. Bruneton, and V. Maupin (2006), Lithospheric and sublithospheric anisotropy beneath the Baltic shield from surface-wave array analysis, *Earth and Planetary Science Letters*, 244(3-4), 590-605.
- Plomerov, J., D. Kouba, and V. Babuska (2002), Mapping the lithosphere-asthenosphere boundary through changes in surface-wave anisotropy, *Tectonophysics*, 358(1-4), 175-185.
- Reiter, K., O. Heidbach, D. Schmitt, K. Haug, M. Ziegler, and I. Moeck (2014), A revised crustal stress orientation database for Canada, *Tectonophysics*, 636(0), 111-124, doi:<http://dx.doi.org/10.1016/j.tecto.2014.08.006>.
- Ross, G. M. (2002), Evolution of Precambrian continental lithosphere in Western Canada: results from Lithoprobe studies in Alberta and beyond, *Canadian Journal of Earth Sciences*, 39(3), 413-437, doi:10.1139/e02-012.
- Ross, G. M., D. W. Eaton, D. E. Boerner, and W. Miles (2000), Tectonic entrapment and its role in the evolution of continental lithosphere: An example from the Precambrian of western Canada, *Tectonics*, 19(1), 116-134, doi:10.1029/1999TC900047.
- Ross, G. M., R. R. Parrish, M. E. Villeneuve, and S. A. Bowring (1991), Geophysics and geochronology of the crystalline basement of the Alberta Basin, western Canada, *Canadian Journal of Earth Sciences*, 28(4), 512-522, doi:10.1139/e91-

045.

Savage, M. K. (1999), Seismic anisotropy and mantle deformation: What have we learned from shear wave splitting?, *Reviews of Geophysics*, 37(1), 65-106, doi:10.1029/98RG02075.

Shearer, P. M., and J. A. Orcutt (1986), Compressional and shear wave anisotropy in the oceanic lithosphere - the Ngendei seismic refraction experiment, *Geophysical Journal International*, 87(3), 967-1003, doi:10.1111/j.1365-246X.1986.tb01979.x.

Shragge, J., M. G. Bostock, C. G. Bank, and R. M. Ellis (2002), Integrated teleseismic studies of the southern Alberta upper mantle, *Canadian Journal of Earth Sciences*, 39(3), 399-411, doi:10.1139/e01-084.

Silver, P. G. (1996), SEISMIC ANISOTROPY BENEATH THE CONTINENTS: Probing the Depths of Geology, *Annual Review of Earth and Planetary Sciences*, 24(1), 385-432.

Smith, M. L., and F. A. Dahlen (1973), The Azimuthal Dependence of Love and Rayleigh Wave Propagation in a Slightly Anisotropic Medium, *J. Geophys. Res.*, 78, doi:10.1029/JB078i017p03321.

Thorkelson, D. J., J. K. Madsen, and C. L. Slaggett (2011), Mantle flow through the Northern Cordilleran slab window revealed by volcanic geochemistry, *Geology*, 39(3), 267-270, doi:10.1130/g31522.1.

Vinnik, L. P., L. I. Makeyeva, A. Milev, and A. Y. Usenko (1992), Global patterns of

Jeff Gu 2015-7-7 3:11 PM

Formatted: Indent: Left: 0 cm, First line: 0 ch

azimuthal anisotropy and deformations in the continental mantle, *Geophysical Journal International*, 111(3), 433-447, doi:10.1111/j.1365-246X.1992.tb02102.x.

West, J. D., M. J. Fouch, J. B. Roth, and L. T. Elkins-Tanton (2009), Vertical mantle flow associated with a lithospheric drip beneath the Great Basin, *Nature Geosci*, 2(6), 439-444, doi:http://www.nature.com/ngeo/journal/v2/n6/supinfo/ngeo526_S1.html.

Xu, Z., X. Song, and S. Zheng (2013), Shear velocity structure of crust and uppermost mantle in China from surface wave tomography using ambient noise and earthquake data, *Earthq Sci*, 26(5), 267-281, doi:10.1007/s11589-013-0010-7.

Yao, H., R. D. van der Hilst, and J.-P. Montagner (2010), Heterogeneity and anisotropy of the lithosphere of SE Tibet from surface wave array tomography, *Journal of Geophysical Research: Solid Earth*, 115(B12), B12307, doi:10.1029/2009JB007142.

Yao, H. J., R. D. van der Hilst, and M. V. de Hoop (2006), Surface-wave array tomography in SE Tibet from ambient seismic noise and two-station analysis - I. Phase velocity maps, *Geophysical Journal International*, 166(2), 732-744.

Yuan, H., and B. Romanowicz (2010), Lithospheric layering in the North American craton, *Nature*, 466(7310), 1063-1068, doi:<http://www.nature.com/nature/journal/v466/n7310/abs/nature09332.html#supplementary-information>.

Zandt, G., A. M. Frassetto, J. F. Cassidy, and M. G. Bostock (2009), Regional variations of mantle anisotropy across the Canadian Cordillera from teleseismic shear-wave splitting, in *American Geophysical Union, Fall Meeting*, edited, San Francisco.

Zhang, P.-Z., et al. (2004), Continuous deformation of the Tibetan Plateau from global positioning system data, *Geology*, 32(9), 809-812, doi:10.1130/g20554.1.

Figure Captions

Fig. 1. Topography map of the study region showing main crustal domains with broadband seismic stations and SKS splitting measurements superimposed. Blue dots are Alberta Telemetered Seismic Network, green diamonds are stations from CRANE array, red dots show Canadian National Seismic Network, and blue diamonds show stations from USArray. Short bars represent SKS splitting parameters (Blue ones from Currie et al. [2004], red ones from Zalt et al. [2009], purple ones from Shragge et al. [2002], white ones from Courtier et al. [2010]). For stations WALA and EDM, the blue and green bars present the splitting parameters for the upper and lower anisotropic layers, respectively [Currie et al., 2004]. Black circles specify null splitting measurements. Black lines show the boundaries of crustal domains beneath the Western Canada Sedimentary Basin. Na-

Nahanni; FS-Fort Simpson; Ho-Hottah; GB-Great Bear; KC-Ksituan and Chincaga; BHT-Buffer Head terrane; Ta-Taltson; Wa-Wabamun; Th-Thorsby; Ri-Rimbey; La-Lacombe; Lo-Loverna Block; VS-Vulcan Structure; EH-Eyehill High; MHB-Medicine Hat Block; STZ-Snowbird Tectonic Zone; GSLsz-Great Slave Lake shear zone.



Fig. 2. Isotropic checkerboard reconstruction result for 50 s period.

Fig. 3. Anisotropic checkerboard reconstruction for 50 s period. (a) checkerboard model of azimuthal anisotropy; and (b) recovery of azimuthal anisotropy.

Fig. 4. Leakage tests based on phase-velocity map at 70 s period. (a) result from isotropic component only. (b) result from anisotropic component only.

Fig. 5. Inversion results of isotropic phase velocities and azimuthal anisotropy for the study region. The isotropic phase velocity is plotted relative to the average phase velocity at the corresponding period. The black bars show the peak-to-peak magnitude and fast propagation direction of azimuthal anisotropy.

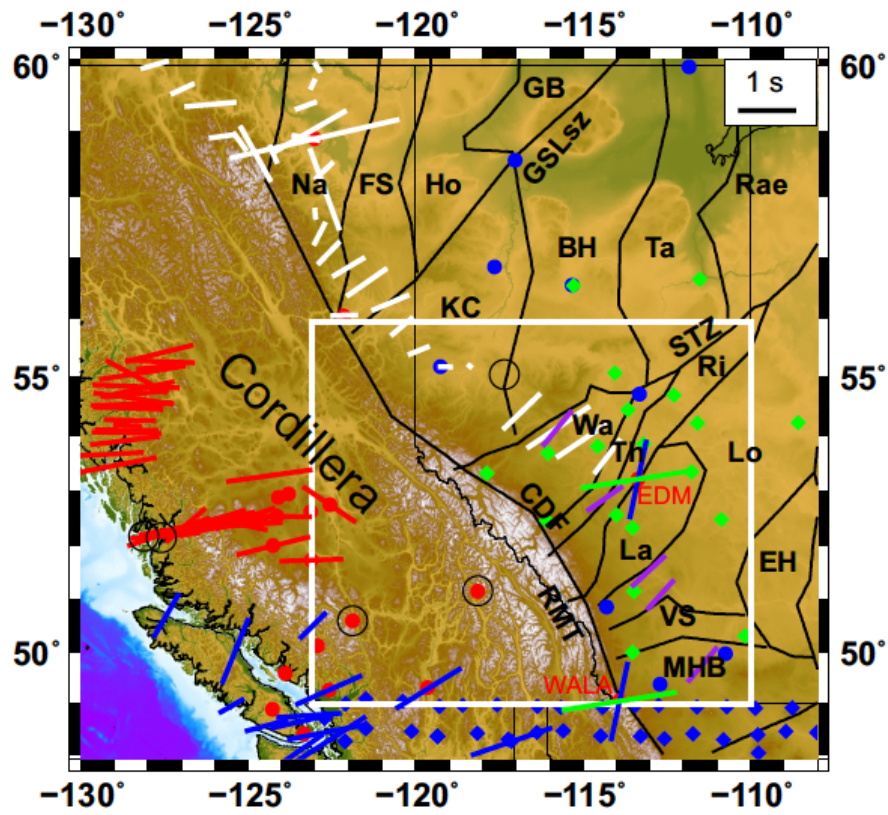


Fig. 1.

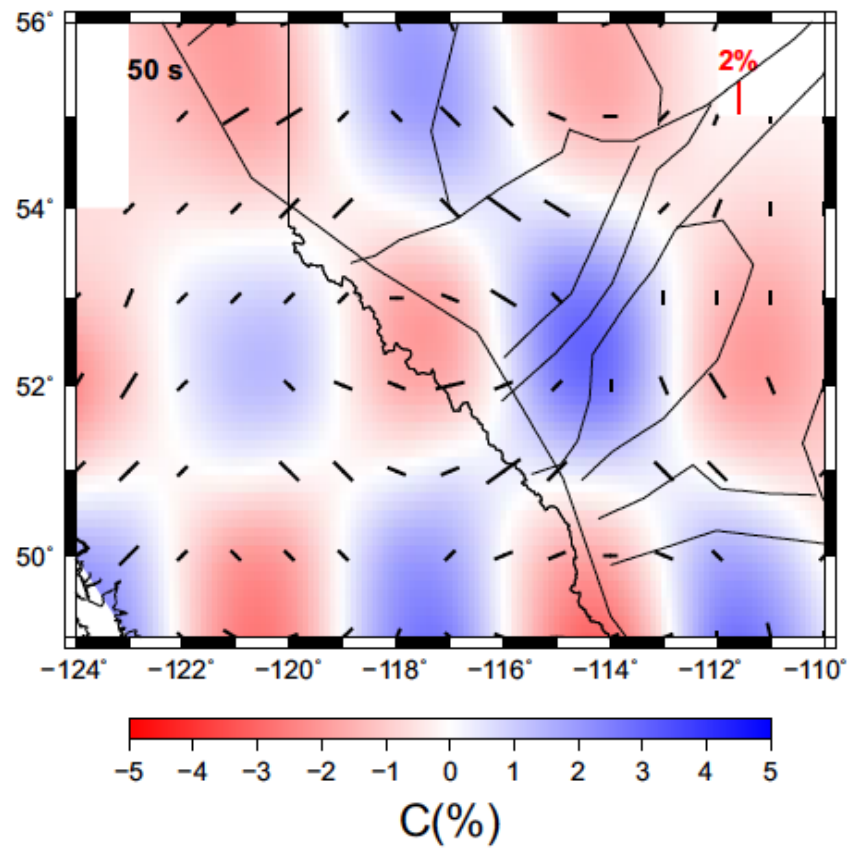


Fig. 2.

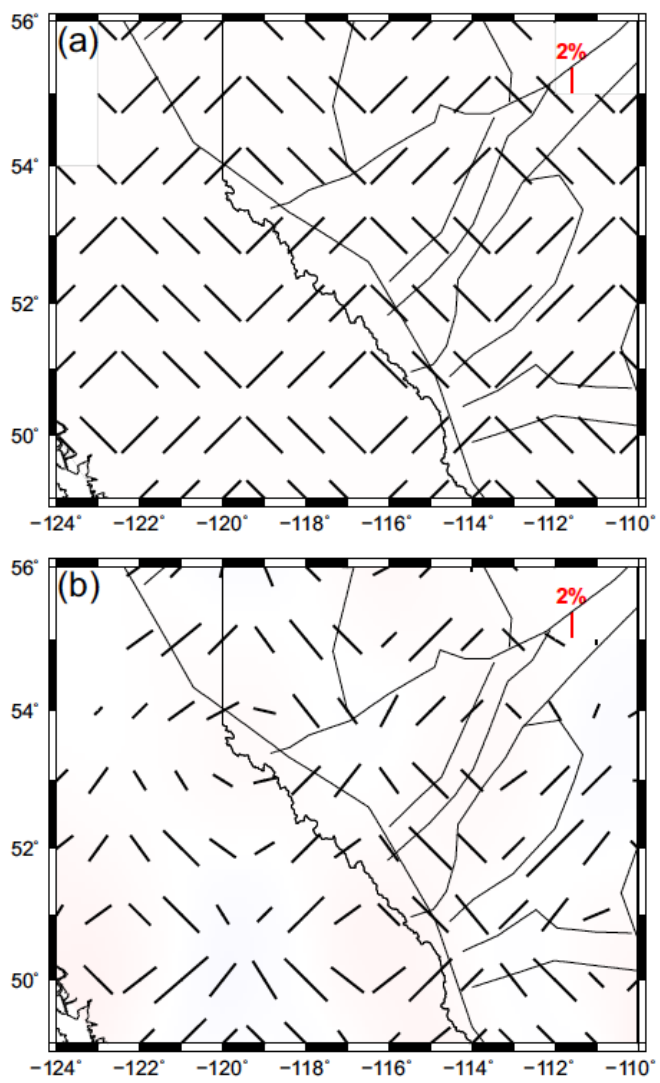


Fig. 3.

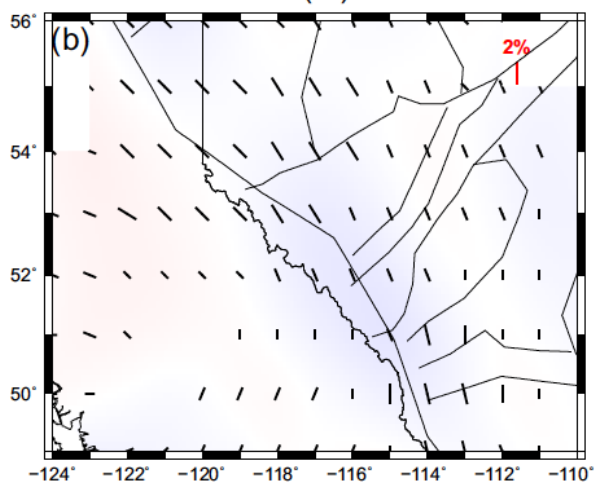
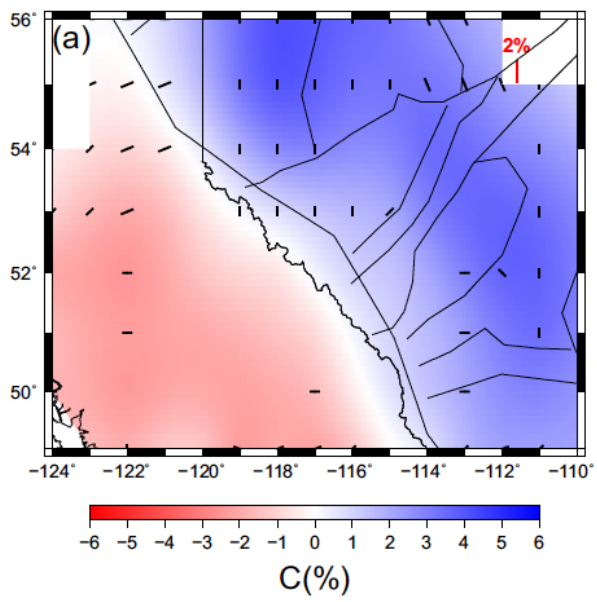


Fig. 4.

Fig. 5.

